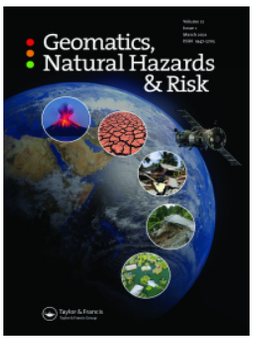

Geomatics, Natural Hazards and Risk

ISSN: (Print) (Online) Journal homepage: https://www.tandfonline.com/loi/tgnh20

Quantitative assessment of ground deformations for the risk management of petroleum and gas pipelines using radar interferometry

Emil Bayramov, Manfred Buchroithner & Martin Kada

To cite this article: Emil Bayramov, Manfred Buchroithner & Martin Kada (2020) Quantitative assessment of ground deformations for the risk management of petroleum and gas pipelines using radar interferometry, Geomatics, Natural Hazards and Risk, 11:1, 2540-2568, DOI: 10.1080/19475705.2020.1853611

To link to this article: https://doi.org/10.1080/19475705.2020.1853611

Published online: 07 Dec 2020.

GEOMATICS, NATURAL HAZARDS AND RISK
2020, VOL. 11, NO. 1, 2540–2568
https://doi.org/10.1080/19475705.2020.1853611

Quantitative assessment of ground deformations for the risk management of petroleum and gas pipelines using radar interferometry

Emil Bayramov[a,b], Manfred Buchroithner[c] and Martin Kada[b]

[a]School of Mining and Geosciences, Nazarbayev University, Nur-Sultan, Kazakhstan; [b]Institute of Geodesy and Geoinformation Science, Technical University of Berlin, Dresden, Germany; [c]Institute for Cartography, Dresden University of Technology, Berlin, Germany

ABSTRACT

The primary objective of these studies was to quantitatively assess the ground deformation velocities and rates and their natural and man-made controlling factors as the potential risks along the seismically active 70 km section of buried Baku-Tbilisi-Ceyhan Oil, South Caucasus Gas, Western Route Oil and South Caucasus Pipeline Expansion Gas pipelines in Azerbaijan using Persistent Scatterer Interferometric Synthetic Aperture Radar (PS-InSAR) technique.

PS-InSAR analysis showed that the continuous subsidence was prevailing in the kilometer range of 13-70 of pipelines crossing two active seismic faults. The ground uplift deformations were observed in the pipeline kilometer range of 0-13. The minimum and maximum vertical ground movement velocities were observed to be −21.3 mm/y and 14.1 mm/y along 70 km section of pipelines with 250 m buffer zone. Both of these sites were observed at the range of seismic faults. The spatial distribution of sites with ground deformation velocity less than −15 mm/y and more than 15 mm/y was diverse and random all along 70 km of pipelines without any cumulative spatial patterns.

Based on the lower mean, variation and standard deviation of pixel values, the seismic fault in the kilometer range of 21-31 revealed its higher vulnerability to subsidence processes rather than the Seismic Fault in the kilometer range of 46-54. The ground deformation velocities within the range of Seismic Fault KP21-31 revealed the minimum and maximum values of −19.74 mm/y and 14.1 mm/y, respectively whereas at the Seismic Fault KP46-54, the minimum and maximum values were −17.07 mm/y and 9.29 mm/y, respectively.

Encouraging level of agreement with the regression coefficients of 0.92 and 0.96 for known subsiding sites at KP28 + 500 and KP52 + 750 and 0.97 and 0.96 for known uplifting sites at KP04 + 900 and KP35 + 050 respectively was observed between the high-precision GPS and PS-InSAR measurements.

The diverse spatial distribution and variation of ground movement processes along pipelines demonstrated that general geological and geotechnical understanding of the study area is not

ARTICLE HISTORY
Received 2 June 2020
Accepted 14 November 2020

KEYWORDS
PS-InSAR; remote sensing; geospatial; pipelines; oil and gas; radar; interferometry; OBIA; machine learning; nearest neighborhood classification

CONTACT Emil Bayramov emil.bayramov@nu.edu.kz

sufficient to find and mitigate all the critical sites of subsidence and uplifts for the pipeline operators. The prediction of the potential subsidence or uplift locations based on the field visual verifications holds a lot of uncertainties without broad and detailed scale airborne and satellite space observation technologies. The justification of the budget for the geotechnical maintenance activities along long-range oil and gas pipelines requires sophisticated prioritization and planning of the remediation sites and clear quantitative and qualitative risk assessment proving the activeness of these sites and effectiveness of the remediation measures. This means that the PS-InSAR – based approach outlined in this paper is a significant improvement over current ground-based monitoring practices or can significantly contribute them in the initial phase of risk assessment and prioritization.

1. Introduction

Ground movement (subsidence or uplift) of just a few centimeters is a serious risk for petroleum and gas pipelines in Azerbaijan-Georgia-Turkey region. If it is not detected timely, the stress on the pipe structure may result in a small leak and major rupture with high consequences to the nearby communities and environmental sensitivities. Ground movement is characteristic to the areas with unstable geology and with high level of anthropogenic impact of subsurface fluid extraction or injection.

The general objective of this study is to quantitatively assess the ground deformations, their natural and man-made controlling factors as the potential risks along buried Baku-Tbilisi-Ceyhan Oil (BTC), South Caucasus Gas (SCP), Western Route Oil (WREP) and South Caucasus Pipeline Expansion Gas (SCPX) pipelines in Azerbaijan. Detailed research goals are following:

1. Detect ground deformation velocities and rates along buried oil and gas pipelines over the period of 2017–2019
2. Determine natural and anthropogenic factors controlling these ground movements
3. Quantification of ground deformation velocity classes with the landcover classes
4. Evaluate the benefits of PS-InSAR remote sensing approach for the geotechnical quantitative risk assessment of surface deformations along pipelines

BTC, WREP, SCP and SCPX pipelines pass through Azerbaijan, Georgia and Turkey and cross wide range of geology, soil, and climate conditions. This obviously creates operational risks for the pipeline operators in the transportation process of petroleum and gas products. Therefore regular quantitative and qualitative risk assessment and mitigation of geotechnical risks for the integrity of pipelines is inevitable to ensure their safe operations. Early warning of ground movement - vulnerable areas contribute to efficient use of geotechnical resources for the cost reduction and safety.

Radar satellite monitoring is the globally proved technology for the cost-effective monitoring, quantitative and qualitative risk assessment and detection of surface movements and prediction of geotechnical hazards independent on weather and lightning conditions. The traditional geodetic ground movement monitoring techniques

are mainly based on conventional geodetic measurements (tacheometry, leveling, and GPS geodesy) which are highly-precise but limited to discrete points, time consuming, expensive field survey activities and limited historical baseline for continuation of measurements.

Nowadays pipeline operators use radar and optical remote sensing to detect third party interference caused by construction or agricultural activities, illegal hottaping and product theft and geohazards like landslides, subsidence or uplift of seismic faults or mud volcanoes, erosions and eroding river crossings. A number of studies were published focused on the prediction of erosion-vulnerable areas along these pipelines in Azerbaijan (Bayramov 2013). However, the quantitative assessment of ground deformation processes (subsidence or uplift) using radar technologies has been studied for some small pipeline terminals and landslide areas of BTC, SCP, WREP and SCPX pipelines. Those studies were primarily performed for commercial purposes making them not accessible for public audience.

There are many studies on the application of InSAR technology for petroleum and gas, mining and also transportation networks (Colesanti et al. 2003; Rucker et al. 2013; Ji et al. 2016; Liu et al. 2016; Mikhailov et al. 2018; Wasowski et al. 2018; Chang et al. 2019; Ru et al. 2019; Shi et al. 2019; Yang et al. 2019; 2019; Zhang et al. 2018, 2019; Zheng et al. 2019,; Yan et al. 2020). There are a limited number of studies focused on the application of InSAR for the measurements of surface motion in pipeline areas (Singhroy et al. 2007, 2015; Sircar et al. 2004; Hole et al. 2011; Guthrie et al. 2018).

To the extent of our knowledge, there are no deep scientific investigations and published papers focused on the use of interferometric technologies for the petroleum and gas pipelines in Azerbaijan, Georgia and Turkey. Most of them were performed within the commercial framework for some pipeline areas without a public access to a society. The novel aspects of the present studies are based on the coupling of interferometric measurements from radar images with advanced geospatial interpolation analysis of measured point cloud for ground deformation velocities and rates. This allowed to detect spatial patterns, hotspots and trends of ground movement along pipelines.

The present studies hold the practical scientific and business values for the petroleum and gas industry with the focus on pipeline operators. The prediction, well-justified investment and mitigation of risks require the combined quantitative and qualitative assessment of actual ground movements and evaluation of potential consequences. Another practical value is the ability to remotely monitor ground movements reducing amount of expensive, time-consuming and dangerous field works (Hole et al. 2011). The remote SAR measurements would significantly contribute to the correlation analysis of space monitoring results with regular inline inspections of the underground pipelines or any other types of in-situ geotechnical measurements. It is obvious that in case of above-ground pipelines, applied interferometric technology will provide remote deformation measurements for both ground and pipelines. However, this research is focused on the buried oil and gas pipelines and it is almost impossible to make any conclusions in terms of the condition of pipelines.

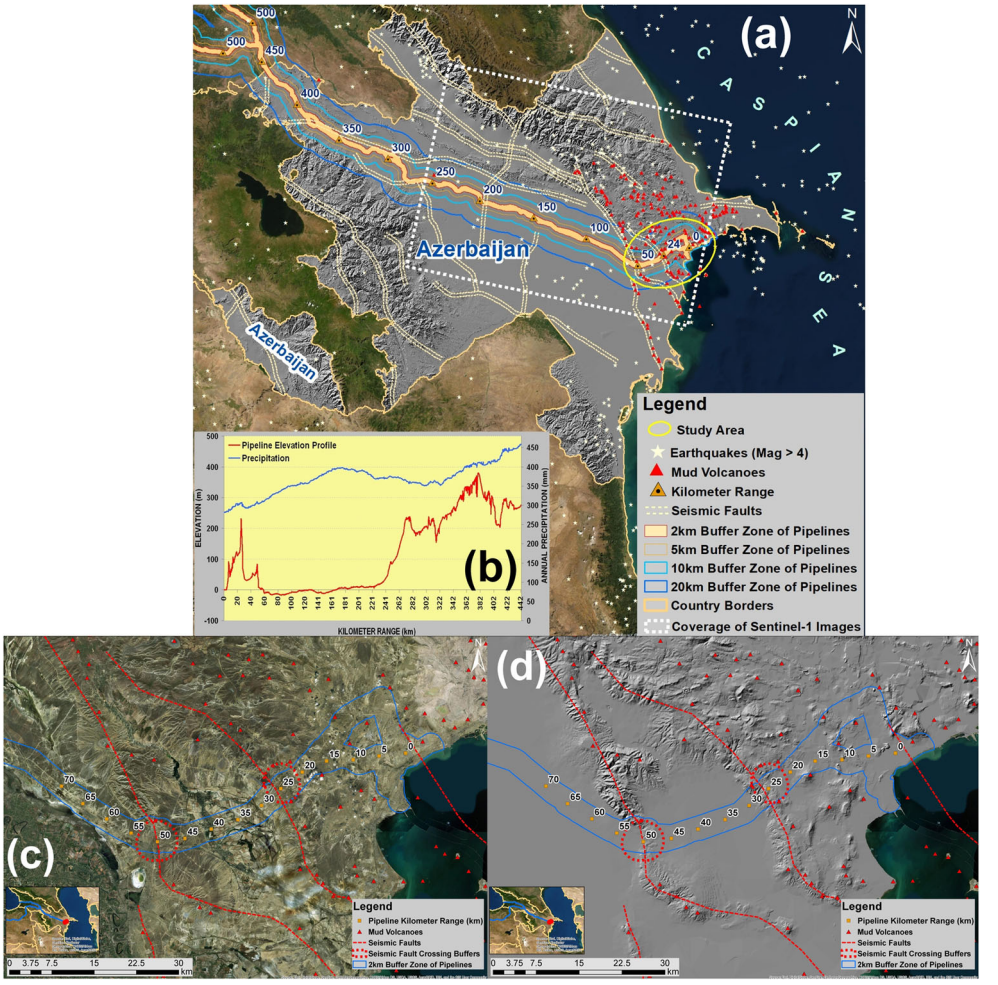

Figure 1. (a) Map of corridors of BTC, SCP, WREP and SCPX pipelines with the indication of seismic faults, earthquakes, mud volcanoes; (b) pipeline profile with precipitation; (c) detailed map of study areas with the worldview-2 satellite imagery background; (d) detailed map of study areas with the hillshaded terrain background.

2. Materials and methods

2.1. Study area

The corridor of BTC oil, SCP gas, WREP oil and SCPX gas pipelines starts at the Sangachal Terminal in Azerbaijan, crosses Georgia and terminates at the Turkey Ceyhan Marine Terminal (Figure 1a). BTC pipeline is 1768 km long (443 km in Azerbaijan, 249 km in Georgia and 1076 km in Turkey). SCP pipeline is a 692 km long (443 km in Azerbaijan and 249 km in Georgia), WREP pipeline is 829 km long (455 km in Azerbaijan and 374 km in Georgia) and SCPX pipeline is 489 km long (424 km in Azerbaijan, 63 km in Georgia and 2 km in Trans-Anatolian Natural Gas Pipeline (TANAP) interconnection). The pipelines pass through areas of active seismic faults in Azerbaijan, Georgia and Turkey (Bayramov 2013). BTC, SCP and SCPX pipelines are properly earthquake engineered through the design of trapezoidal trenches to reduce

soil resistance either side of the pipe to allow it to move more freely in case of significant ground movements whereas WREP pipeline is quite old and was designed based on the lower protection principles against ground movements.

The present research focused on the pipeline corridors of Azerbaijan section within 0-70 km range (Figure 1a). This range of pipelines crosses most active seismic faults at KP25 and KP50. The depth of the buried pipelines varies between 1-2.5 meters, whereas at the rivers, roads, rails and seismic faults it can reach up to 31 meters. Ground water level varies in the range of 3-8 meters increasing from west to east. The average precipitation along this section of pipelines is 150-250mm (Figure 1b). The precipitation increases from east to west because of the elevation factor along the right of way of pipelines. The average annual air temperature along pipelines is 15 °C. This section of pipelines is characterized by silt loam, silty clay, silty clay loam, clay loam, clay, sandy clay loam with hilly terrain. The spatial distribution of soil types with silt content and hilly terrain prevails in the majority of areas what makes this section of pipelines vulnerable to erosion processes (Bayramov 2013). Soil moisture increases from east to west and is variable in the range of 3-15% because towards west more agricultural activities take place (Figure 1c and d).

2.2. Quantitative assessment of ground deformations along petroleum and gas pipelines using PS-InSAR

PS-InSAR is a proven differential interferometric technique which involves processing of multi-temporal Synthetic Aperture Radar (SAR) data to identify persistently reflecting ground features and their motion rates with a millimeter-level precision (Ferretti et al. 2001; Hooper et al. 2004; Kampes 2005; Perissin and Ferretti 2007; D'Aria et al. 2010; Honglei and Jun-Huan 2015). High - density and - accuracy PS-InSAR - derived surface deformation measurements acquired over wide range of areas and longtime periods obviously qualify this technique for the risk management of above-ground and buried petroleum and gas pipelines (Ianoschi et al. 2013). Therefore, PS-InSAR is a cost-effective tool that contributes to the prediction and mitigation of geotechnical and geological risks what is crucial for safe, simplified and optimized operation and maintenance of petroleum and gas assets (Ferretti et al. 2000; 2005; 2007; 2011).

The PS-InSAR concept for the measurement of precise displacement is based on finding of permanent scatters with phase stability over a long period of time, removal of atmospheric phase contribution, DEM error and system/thermal noise etc. (Lu and Liao 2008). The advantage of PS-InSAR technique is that it overcomes the problems of geometrical and temporal decorrelation by using a large number of radar images (Lu and Liao 2008). However, it is necessary to emphasize that the applicability and quality of InSAR technology depends on the scale of study area and type of infrastructure. Therefore in some specific cases of detailed infrastructure monitoring this technology may not be selected as optimal to replace ground-based geodetic measurements (Chang et al. 2018).

For regular and detailed ground deformation risk assessment and maintenance of petroleum and gas assets, it is highly recommended to use highest spatial and temporal resolution radar satellite images (TerraSAR-X, Radarsat-2 or COSMO-SkyMed)

to achieve maximum point density with the highest possible horizontal and vertical precision. Unfortunately, only accessible source of radar images for the present studies were Sentinel 1 A and Sentinel 1B which are free accessible to the research community from the European Space Agency (ESA).

Monitoring and characterization of ground deformation processes along 70 km section of oil and gas pipelines have been carried out by using a stack of total of 59 Sentinel-1 satellite images using PS-InSAR technique. The spatial coverage of Sentinel-1 radar satellite images is presented in Figure 1a. Sentinel-1 satellite images were acquired in C-band (wavelength 5.55 cm) with a revisiting time of 6 days considering both satellites (1 A and 1B). The images in interferometric wide swath mode provide a wide spatial coverage of about 250 km with a slant range resolution of 5 m and an azimuth resolution of 20 m (Yang et al. 2019). The radar images cover the period January 2018 - December 2019 and have been acquired in descending orbit with VV + VH polarizations, IW beam mode, Path − 6 and Absolute Orbit − 29828. Sentinel − 1 VV polarization bands were used since co-polarized bands provide higher coherency (Imamoglu et al. 2019).

Low temporal baseline of Sentinel-1 contributed to the prevention of significant temporal decorrelations in the coherency of pixels (Solari et al. 2020). Accuracy and precision of the computed surface displacements are limited by the decorrelation of the SAR signals, the atmospheric delays and the phase-unwrapping error (Yunjun et al. 2019). The following workflow shown in Figure 2 was used for PS-InSAR, geospatial interpolations, object-based remote sensing classification and statistical analysis.

The main processing steps of PS-InSAR consist of interferogram generation, multitemporal persistent scatterers (PSI) processing and removal of atmospheric phase screen (Osmanoğlu et al. 2016). Shuttle Radar Topography Mission (SRTM) (Farr et al. 2007) with 1 arc-second (∼30 m pixel size) DEM from the National Aeronautics and Space Administration (NASA) and precise orbits from the European Space Agency (ESA) were used for the coregistration and for the topographic phase removal from the interferometric phase (Imamoglu et al. 2019). The resolution of the DEM was sufficient for the removal of the topographical component from the interferograms and calculation of the residual topographic errors (Solari et al. 2020).

PS-InSAR - based generated ground deformation monthly rates were quality controlled using time-series high-precision GPS measurements conducted for two known subsiding positions - KP28 + 500 and KP52 + 750 and two known uplift positions - KP04 + 900 and KP35 + 050 located along the corridor of oil and gas pipelines. Regression analyses were performed to evaluate a correlation between PS-InSAR and ground-based high-precision GPS measurements. The ground-based GPS measurements were performed in parallel with the acquisition of satellite images to eliminate a temporal decorrelation.

The geospatial analyses were used to generate the Point Density and Trend surfaces for the determination of ground deformation spatial patterns along pipelines. Point density surfaces were generated based on the circular neighborhood radius that was defined as the shortest of the width or height of the extent of the input point cloud divided by 30 (ESRI 2014a). This allowed to calculate a magnitude-per-unit

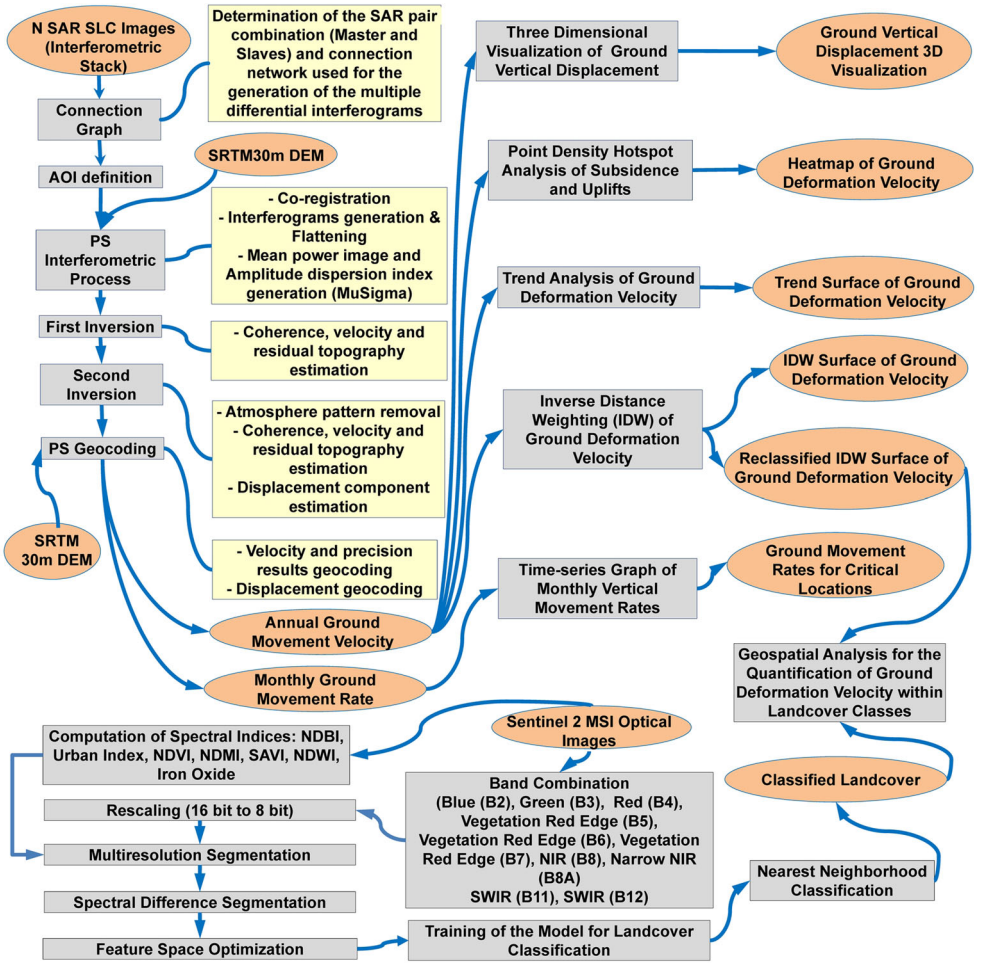

Figure 2. Workflow for PS-InSAR and machine learning – based remote sensing classification of landcover.

area from point features that felt within a neighborhood around each cell. For the generation of trend surfaces, global polynomial interpolation was used to fit a smooth surface defined by a mathematical polynomial function to the input point cloud for the gradual capturing of coarse-scale spatial patterns (ESRI 2014b).

2.3. Machine learning – based object – based landcover classification along petroleum and gas pipelines

Numerous comparative studies determined the limited accuracy and reliability of pixel-based classification with the significant drawback of misclassification and "salt and pepper" effect (Ivits et al. 2005; Yan et al. 2006; Durieux et al. 2008; Dupuy et al. 2012). Object-based image analysis (OBIA) has proven the reliability of its approach to solve this challenge by the segmentation process of homogeneous region to delineate the objects for further classification using spectral and spatial information such

Table 1. The spectral bands, wavelength and spatial resolutions of Sentinel-2 MSI sensor.

Band	Description	Wavelength (μm)	Resolution (m)	Used for Classification
1	Coastal aerosol	0.433 – 0.453	60	
2	Blue	0.458 – 0.523	10	X
3	Green	0.543 – 0.578	10	X
4	Red	0.650 – 0.680	10	X
5	Vegetation Red Edge1	0.698 – 0.713	20	X
6	Vegetation Red Edge2	0.733 – 0.748	20	X
7	Vegetation Red Edge3	0.773 – 0.793	20	X
8	NIR	0.785 – 0.900	10	X
8A	Narrow NIR	0.855 – 0.875	20	X
9	Water vapour	0.935 – 0.955	60	
10	SWIR – Cirrus	1.365 – 1.385	60	
11	SWIR-1	1.565 – 1.655	20	X
12	SWIR-2	2.100 – 2.280	20	X

as texture, shape and context features (Sande et al. 2003; Liu and Xia 2010; Myint et al. 2011). Most comparative studies of pixel - and object - based classification techniques proved that OBIA provides more reliable results (Matinfar et al. 2007; Cleve et al. 2008; Dehvari and Heck 2009; Whiteside et al. 2011).

Therefore, the object-based classification technique was selected for this study to classify the landcover along 70 km long section of pipelines using Sentinel-2 MSI satellite images acquired in August 2019. OBIA in eCognition software was used to produce the following landcover classes: agricultural, grasslands, industrial, volcanoes mud, residential areas, semi-desert areas and water. For the achievement of the best quality of multi-resolution segmentation and classification results, the spectral indices computed from Equation 1-7 and the imagery bands (Blue, Green, Red, Vegetation Red Edge 1, Vegetation Red Edge 2, Vegetation Red Edge 3, NIR, Narrow NIR, SWIR-1, SWIR-2 (Table 1) were used in the segmentation stage to achieve maximum possible spectral separation of segment for different landcover classes. After the Multiresolution Segmentation was generated, Spectral Difference Segmentation was run to dissolve segments of similar spectral, shape and texture characteristics for the simplification and optimization of classification model with the optimal number of segments. Afterwards, the training segments/samples were randomly collected with the consideration of spectral difference so that classification model can distinguish and assign segments to relevant landcover classes. Prior to running of the final Nearest Neighborhood Classification, the Feature Space Optimization was run to optimize the spectral difference of segments through the selection of most appropriate bands and spectral indices contributing to the spectral separation of segments. Quality assurance of the classified land-cover was performed using randomly distributed 650 control points and the standard error (confusion/contingency) matrix. The contextual information of seismic faults, mud volcanoes and historical records of earthquakes were also used to understand how PS-InSAR detected ground deformations are spatially related to the natural tectonic factors.

$$\text{Built}-\text{Up Index (NDBI)} = (\text{SWIR1} - \text{NIR})/(\text{SWIR1} + \text{NIR}) \quad [1]$$

$$\text{Urban Index} = \text{Offset} + \text{Scale} * (\text{NIR} - \text{SWIR2})/(\text{NIR} + \text{SWIR2}) \quad [2]$$

$$\text{Normalized Difference Vegetation Index (NDVI)} = (\text{NIR} - \text{RED})/(\text{NIR} + \text{RED}) \quad [3]$$

$$\text{Normalized Difference Moisture Index (NDMI)} = (\text{NIR} - \text{SWIR1})/(\text{NIR} + \text{SWIR1}) \quad [4]$$

$$\text{Soil Adjusted Veg. Index (SAVI)} = \text{Offset} + \text{Scale} * (1.5 * (\text{NIR} - \text{RED})/(\text{NIR} + \text{RED} + 0.5)) \quad [5]$$

$$\text{Normalized Difference Water index (NDWI)} = (\text{Green} - \text{NIR})/(\text{Green} + \text{NIR}) \quad [6]$$

$$\text{Iron Oxide} = \text{Iron Oxide Ratio} = \text{Red/Blue} \quad [7]$$

3. Results

3.1. Ground deformations detected from PS-InSAR

Over 3.42 million PS points were computed from the processing of the Sentinel-1 radar satellite images for 70 km pipeline range with 10 km buffer zone. As a result of multi-temporal PSI analysis, two main products were produced: (1) ground deformation velocity, and (2) time-series of displacements for measured points. Ground deformation values were calculated relative to a common reference SAR image acquired in January 6, 2018.

PSI analyses enable retrieval of the average Line-Of-Sight (LOS) subsidence or uplift rates (Bonì et al. 2018). For the accurate computation of the vertical velocity from LOS, it is critical to perform the PSI computations from both ascending and descending satellite passes (Aslan et al. 2019). However, it was not possible for the present research because of non-sufficient computing power and storage space for the PSI processing. PSI results in a LOS velocity for each coherent point, towards or away from the satellite and if it is simply assumed that all motion is vertical, the vertical velocity was obtained through dividing the LOS displacement rates by the cosine of the radar incidence angle (Hole et al. 2011; Dai et al. 2015; Gee et al. 2016).

The connection graphs of SAR images in Figures 3a and 3b present that all 59 radar images are well connected in time in order to follow the displacement monitoring over the period of 2018–2019.

Less number of PSI points was measured for croplands because of the temporal decorrelation caused by vegetation cover. The coverage of agricultural lands was increasing from east to west, therefore PSI performed better for the barelands located in the pipeline range of 0-15 km (Figure 3c). For this reason, it was critical to perform the IDW interpolation to cover the gaps in the developed grid model of ground deformations for easier interpretation of surface movements. This obviously caused the uncertainty in the research. However, this would not significantly affect the overall statistical accuracy and reliability of results along the main corridor of pipelines

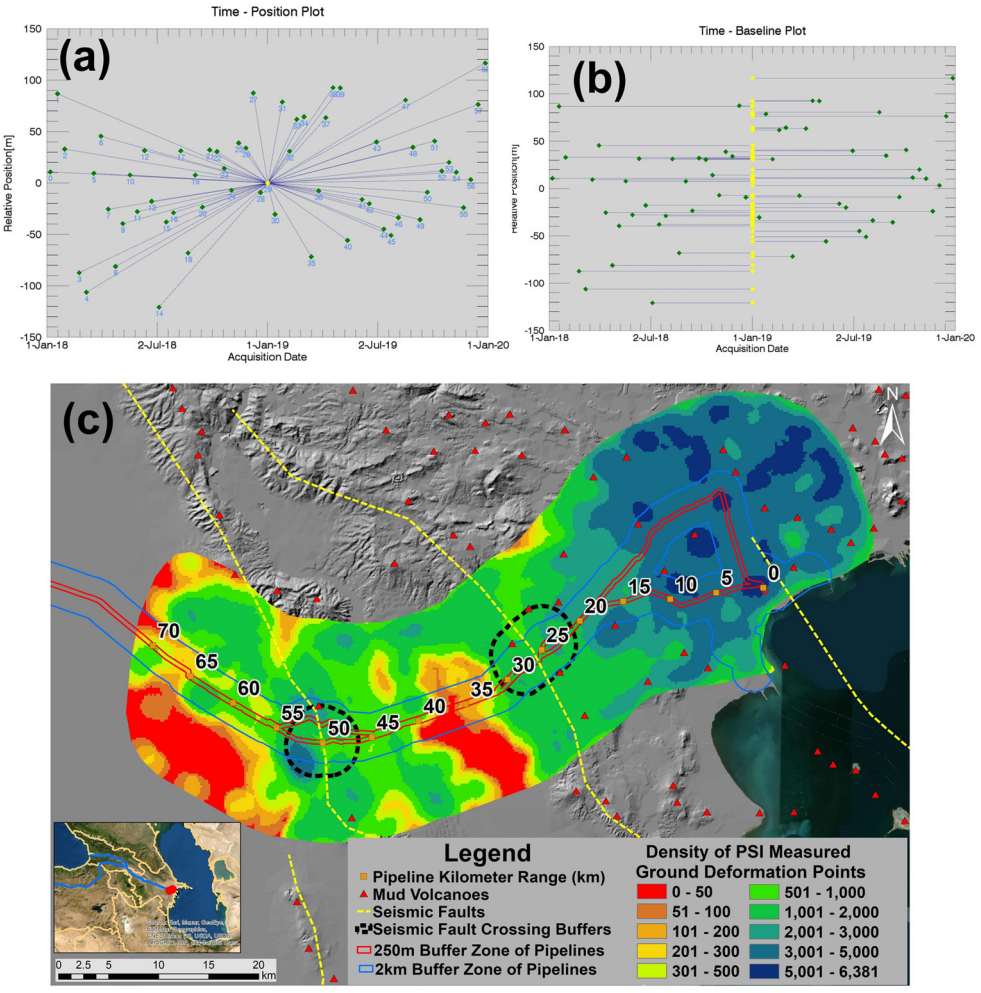

Figure 3. Connection graphs: (a) time-baseline plot for PSI; (b) time - baseline plot for PSI; (c) density of PSI measured points.

with the buffer zone of 250 m that had a sufficient coverage of PSI - measured point cloud (Figure 3c).

Even though the pipeline buffer that is subject to the risk assessment can be variable in the range of 40-500 m, PSI computations for 10 km buffer zone of pipelines were inevitable to understand the large-scale ground deformation patterns of seismic faults along 70 km section of pipelines. Afterwards, the selected two seismic faults were investigated from the local perspectives. PSI computed ground deformation velocity and hotspots of subsidence and uplifts are presented in Figures 4a and 4b, respectively. Negative displacement values are represented by cool colors (shades of blue color) and positive displacement values (shades of brown color) for the period of observations.

From the Figures 4a and 4b, it is possible to observe the extended subsidence patterns in the KP13-70 range. The ground uplift deformations were observed in the

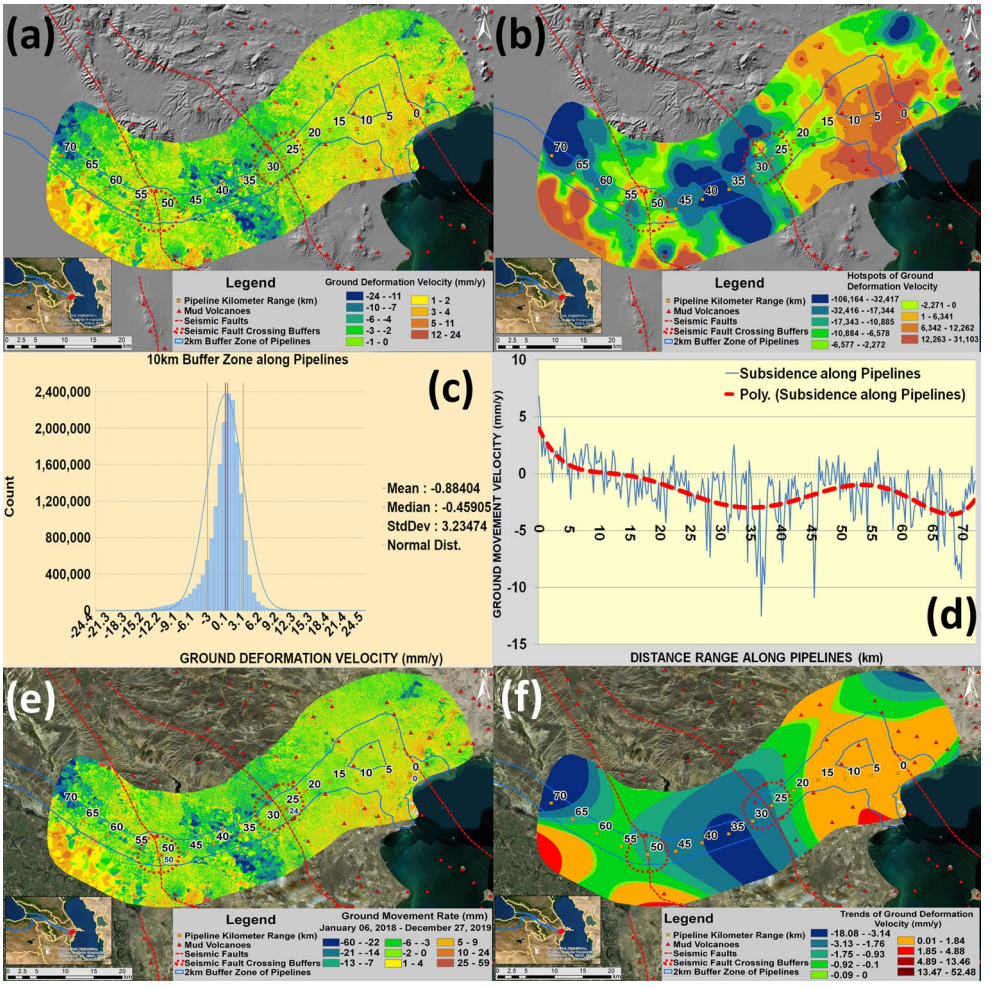

Figure 4. (a) Map of ground deformation velocity along petroleum and gas pipelines; (b) map of hotspots of ground deformations velocity; (c) histogram of ground deformation velocity of 70 km long pipeline section with 10 km buffer zone; (d) profile view of ground deformation velocity for 5 KP interval markers along oil and gas pipelines; (e) map of ground movement rates (January **06, 2018** and December **27, 2019**); (f) map of ground movement trends.

pipeline range of KP0-KP13. The prevailing majority of negative values are also reflected in Figure 4c and the negative mean value is another indicator of the subsiding processes in the study area. From Figure 4d, that represents the profile of ground deformation velocities for 5 km stations along pipelines, it is possible to observe that the most significantly subsiding areas were located in the pipeline range of KP30 - KP45 between two seismic faults and KP60 - KP72. Figure 4e represents the ground deformation rates between January **06, 2018** and December **27, 2019**. The minimal and maximal ground deformation rates over the duration of two years were -60mm and 59 mm, respectively. The trends of the ground deformation velocity showed that there is a clear subsidence process occurring between two seismic faults Figure 4f and the subsidence was increasing towards south. This could also be

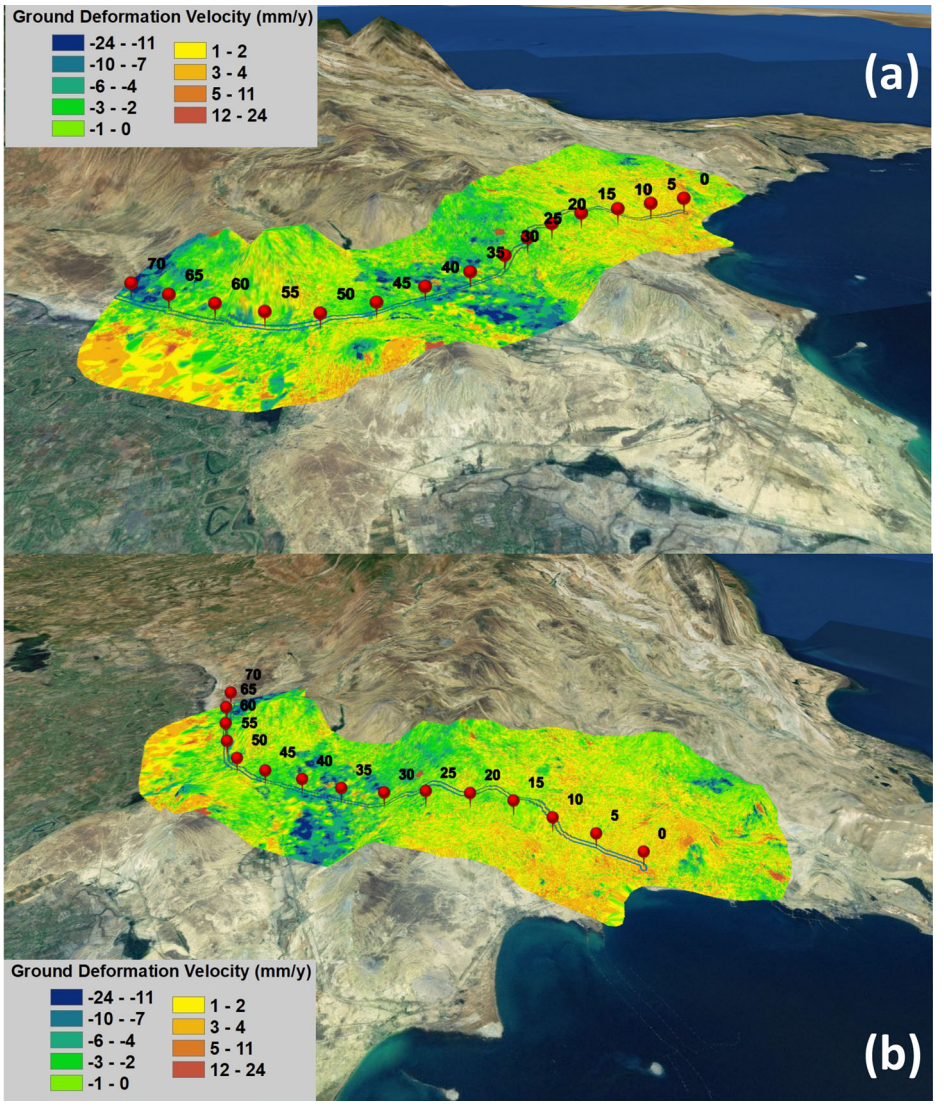

Figure 5. Three-dimensional representation of ground deformation velocities (visual exaggeration: 3 times): (a) south-west view; (b) south-east view.

observed in the three-dimensional representation of ground deformation velocities (Figures 5a and 5b).

Local-scale analyses were performed along 70 km section of pipelines with 250 m buffer zone for the detailed quantitative ground movement assessment of two seismic faults. The minimum and maximum vertical ground movement velocities were observed to be −21.3 mm/y and 14.1 mm/y (Figures 6a and 6b). The histogram in Figure 6b shows that the majority of negative values prevail along 70 km section of pipelines with mean value of ground deformation velocity equal to −1.36 mm/y (Figures 6a and 6b). As it is possible to observe in Figures 6a and 6b, the significant variability of ground deformations was observed along the entire range of pipeline

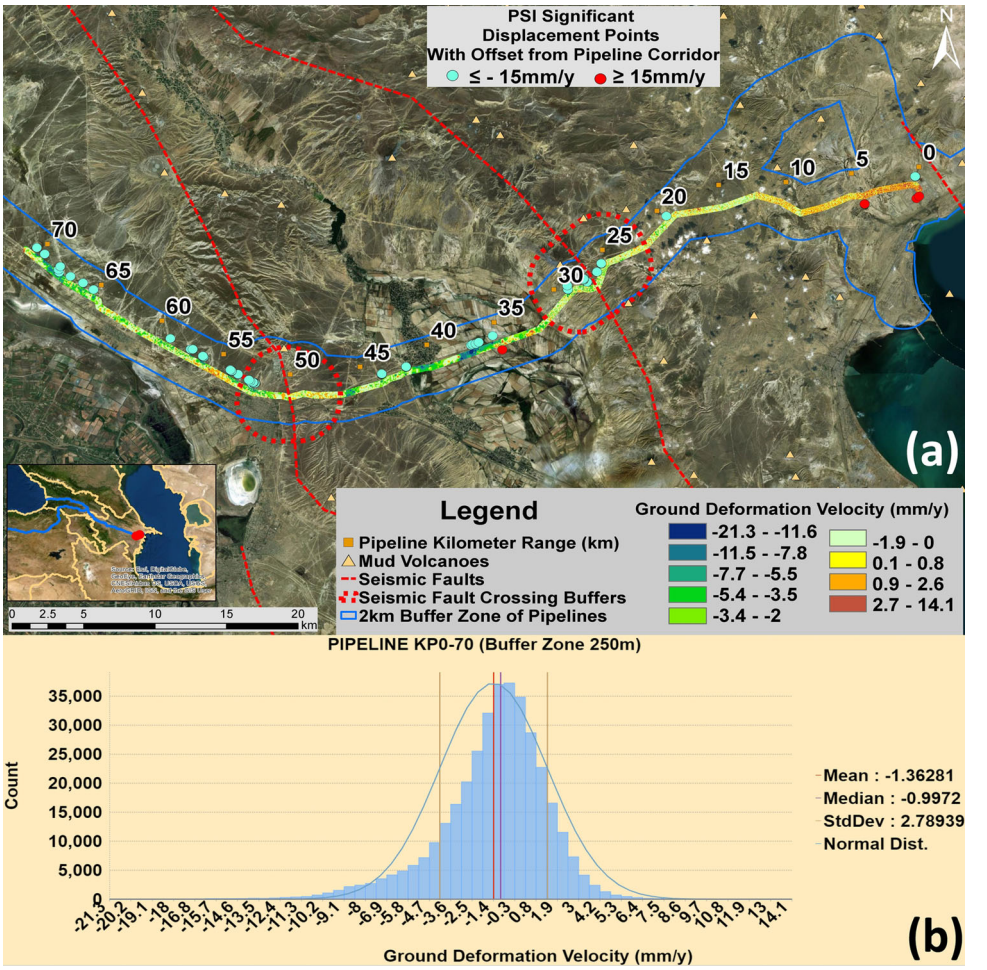

Figure 6. (a) Map of ground deformation velocity; (b) histogram of ground deformation velocity along 70 km petroleum and gas pipelines corridor within 250 m buffer zone.

corridor. In Figure 6a, the PSI points with ground deformation velocity of more than 15 mm/y and less than −15 mm/y also indicated the random distribution of the uplift and subsidence processes along the corridor of petroleum and gas pipelines. Therefore, it is obvious that the prediction of the potential subsidence or uplift locations based on the single geotechnical and geological judgment of the natural hazards holds a lot of uncertainties without broad and detailed scale airborne and satellite space observation technologies. The justification of the budget for the geotechnical maintenance activities along long-range oil and gas pipelines requires sophisticated prioritization and planning of the remediation sites. It also requires the detailed quantitative and qualitative risk assessment proving the activeness of these sites and effectiveness of the remediation measures. The minimum and maximum ground movement rates in December **27, 2019** since January **6, 2018** were observed to be −46.09 mm (KP52 + 620) and 33.46 mm (KP27 + 016), respectively. Both of them

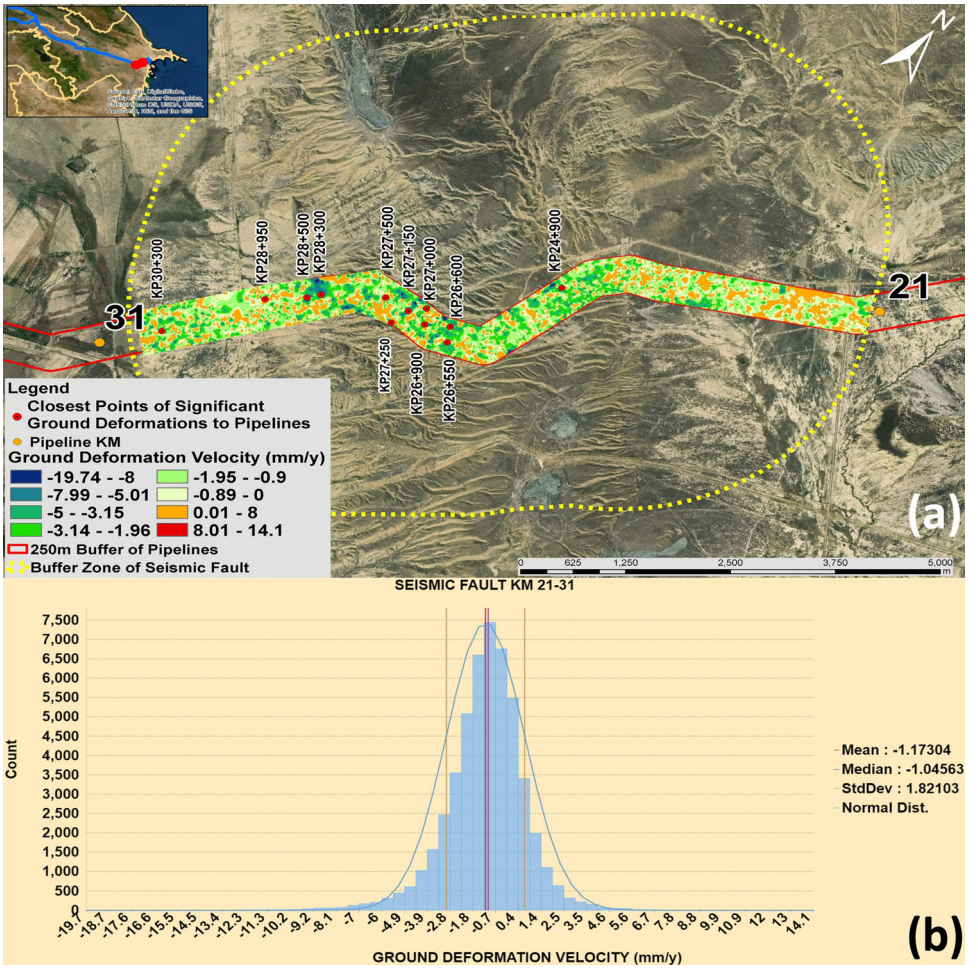

Figure 7. (a) Detailed map and (b) histogram of the ground deformation velocity for 250 m buffer zone of pipeline corridor crossing the seismic faults at KP21-31 range.

were observed within the buffer zones of two seismic faults indicated in Figure 1b and 1c.

The ground deformation velocities within the range of Seismic Fault KP21-31 revealed the minimum and maximum values of −19.74 mm/y and 14.1 mm/y, respectively (Figures 7a and 7b). However, the minimum and maximum ground movement rates in December **27, 2019** since January **6, 2018,** were observed to be − 46.07 mm (KP26 + 900) mm and 33.46 mm (KP27 + 250), respectively. The ground deformation velocities within the Seismic Fault KP46-54 revealed the minimum and maximum values of −17.07 mm/y and 9.29 mm/y, respectively (Figure 8a). However, the minimum and maximum ground movement rates in December **27, 2019** since January **6, 2018,** were observed to be −46.09 mm (KP52 + 750) and 22.24 mm (KP52 + 350), respectively. Based on the histograms in Figures 7b and 8b, it is possible to observe that the mean pixel value of Seismic Fault KP21-31 equal to −1.17 mm is lower than in the Seismic Fault KP46-54 equal to −1.01 mm what allows to assume that the

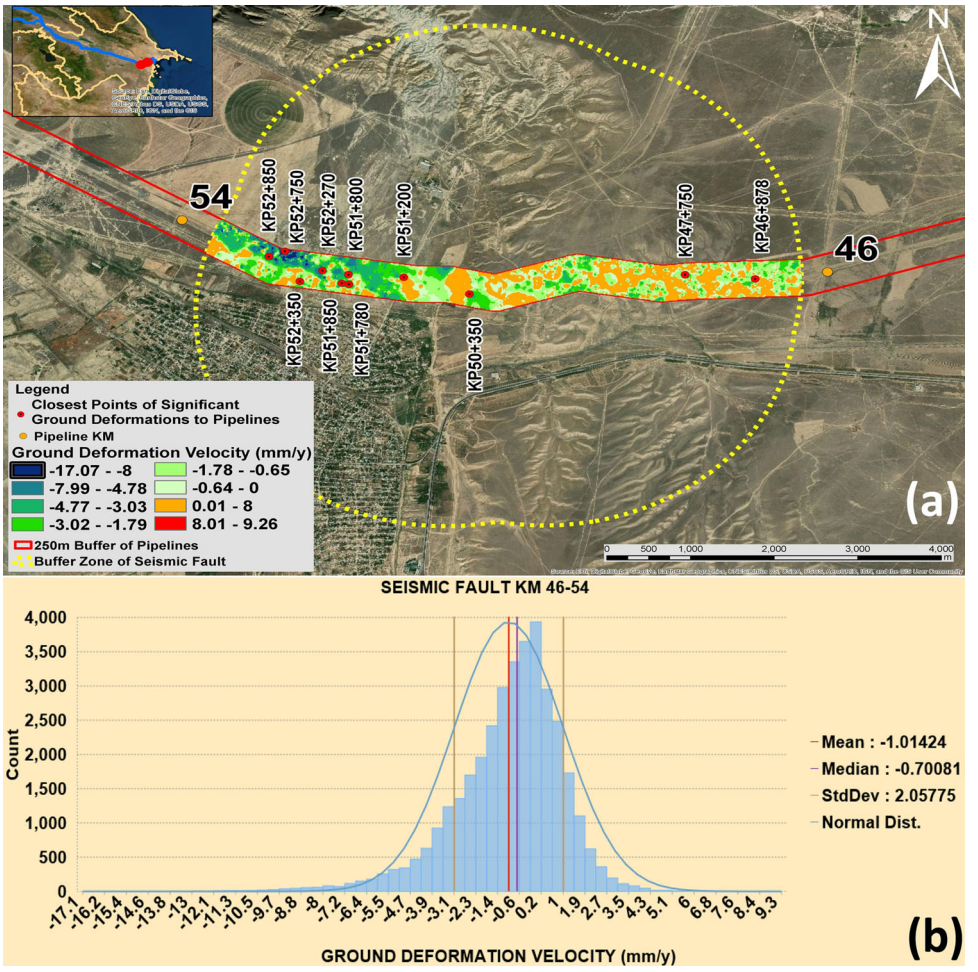

Figure 8. (a) Detailed map and (b) histogram of the ground deformation velocity for 250 m buffer zone of pipeline corridor crossing the seismic faults at KP46-54 range.

subsidence processes prevail in both seismic faults but Seismic Fault KP21-31 is affected by higher rates of negative ground movement. However the Seismic Fault KP46-54 indicated higher standard deviation equal to 2.06 rather than Seismic Fault KP21-31 with the value of 1.82. This allows to assume that the spatial variation of negative and positive values is higher in the Seismic Fault KP46-54, hence both uplifting and subsidence processes prevail in this seismic fault. In Figures 7a and 8a, the most subsiding and uplifting sites were depicted on the maps with the ground movement rates shown in Figures 9a and 9b. It is possible to observe that the critical movement points of Seismic Fault KP21-31 also indicated lower mean value of −9.48 mm rather than in Seismic Fault KP46-54 with the mean value of −8.41 mm. It is also necessary to emphasize the variation of temporal ground deformation rates in all of these critical sites, in spite of the fact that they are not so distant from each other. Figures 10a and 10b also presented the significant variation of ground deformation velocity changes with the mean values of −0.99 mm and −0.95 mm, standard deviation of 1.34 and 1.74, variation of 1.78 and 3.03 in Seismic Faults KP21-31 and

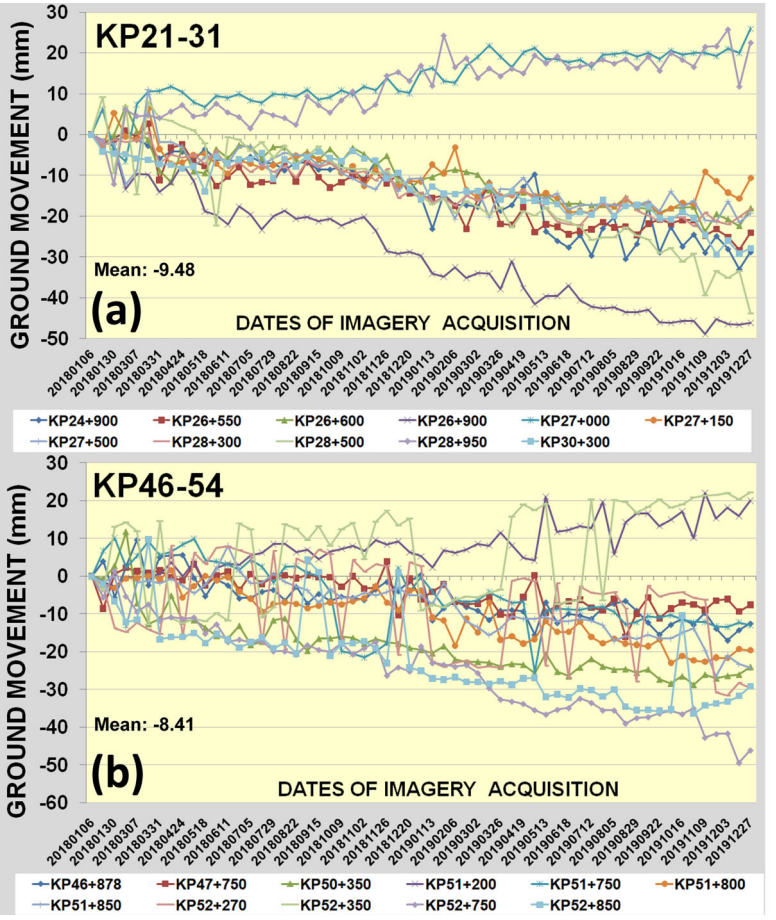

Figure 9. Graphs of ground movement rates for the most significantly subsiding and uplifting points within 250 m buffer zone of pipelines crossing the seismic faults at (a) KP21-31 and (b) KP46-54 ranges.

KP46-54 located along the pipelines, respectively. In this case by lower mean and standard deviation values, Seismic Fault KP21-31 was identified as more vulnerable to subsidence processes whereas the higher variation values in Seismic Fault KP46-54 could be explained by the vulnerability to both uplift and subsidence processes. The detected locations of critical movement points through the significantly variable ground deformation velocities and rates once again proved the complexity of in-situ based visual inspections and geodetic measurements applied often by pipeline operators for the assessment, early warning and mitigation of pipeline risks.

Prior to the implementation of the foregoing geospatial analysis, PS-InSAR measurements were validated using the time-series of high-precision GPS measurements with long-term observations on the ground for two known subsiding positions at KP28 + 500 and KP52 + 750 and for two known uplifting positions at KP04 + 900 and KP35 + 050 (Figures 6a, 7a, 8a, and 11a–d). Encouraging level of agreement with the regression coefficients of 0.92 and 0.96 for KP28 + 500 and KP52 + 750 respectively was observed between the high-precision GPS and PS-InSAR measurements

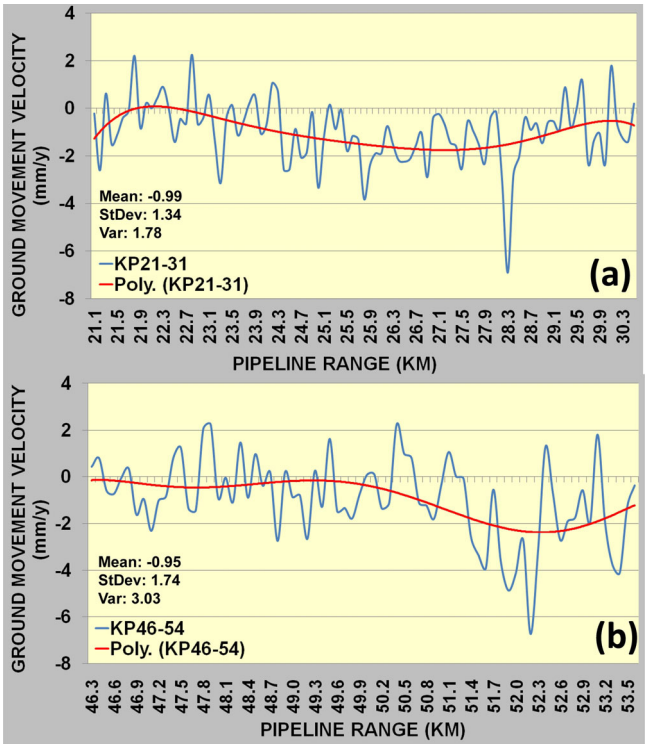

Figure 10. Graphs of ground deformation velocity profiles (10 m stationing interval along pipelines).

(Figure 11a–d). Quality assurance and control revealed the RMSE of 2.7 mm and 2.5 mm for KP28 + 500 and KP52 + 750, respectively. The similar validation was performed for two known uplifting locations with existing historical GPS measurements along pipelines at KP04 + 900 and KP35 + 050 (Figure 11e–h). In this case, it was also possible to observe the encouraging level of correlation between the high-precision GPS and PS-InSAR measurements with the regression coefficients of 0.97 and 0.96 for KP04 + 900 and KP35 + 050, respectively (Figure 11e–h). Quality assurance and control revealed the RMSE of 1.7 mm and 1.9 mm for KP04 + 900 and KP35 + 050, respectively (Figure 11e–h).

Although the GPS measurements showed minor variations in comparison to PS-InSAR, the achieved accuracy allows to state without any doubts that the deformation trends clearly confirmed the presence of subsidence processes at the seismic faults. According to Grebby et al. 2019, the residual discrepancy between two datasets is related to the difference between point-based and areal measurements, LOS cosine corrections, and other variations in the field operating conditions.

3.2. Quantification of ground deformation velocity within the landcover classes

The landcover was developed using the Sentinel-2 MSI sensor satellite images acquired for low-cloudiness time period of August 2019. The object-based classification approach was used for the classification of the following landcover classes:

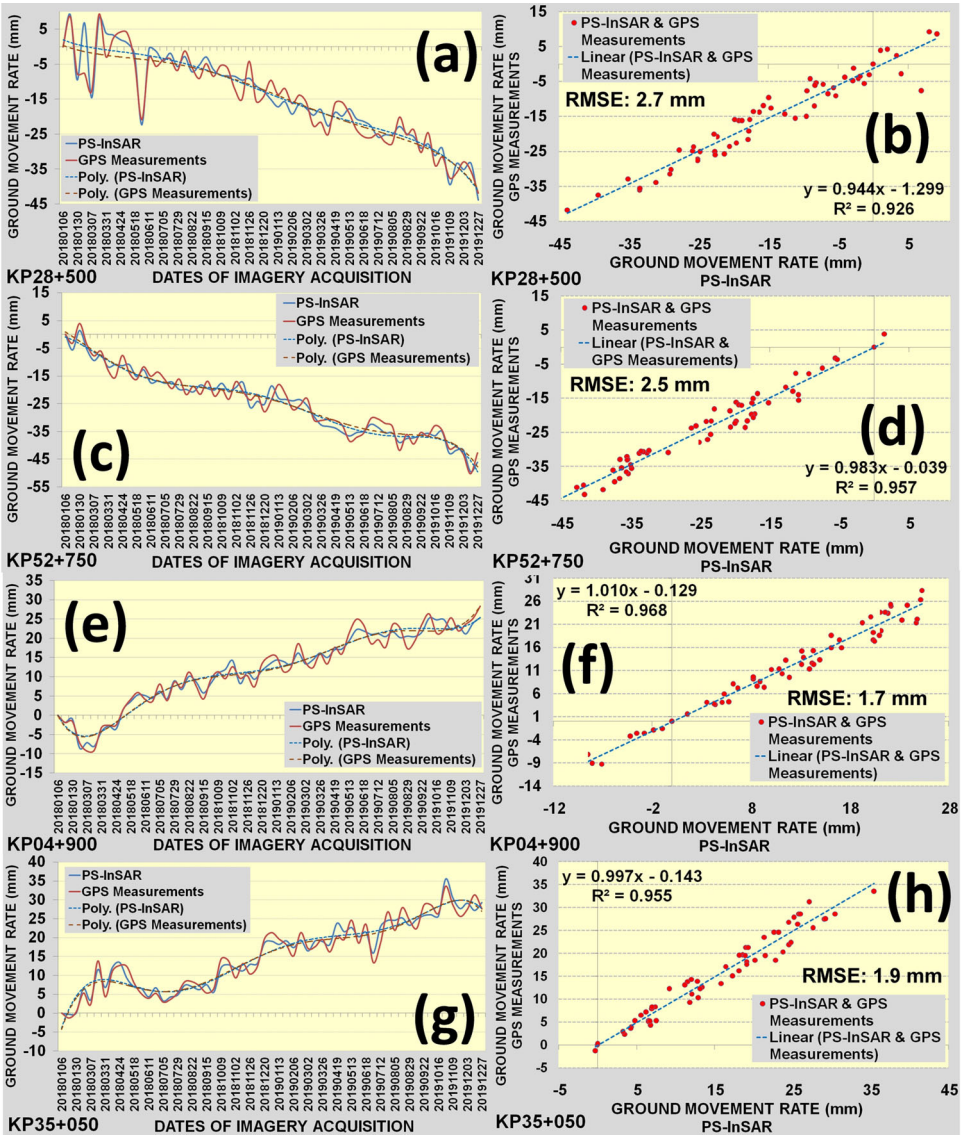

Figure 11. Validation of PS-InSAR ground movement rates using high-precision GPS measurements: (a) line graph for KP28 + 500; (b) regression graph for KP28 + 500; (c) line graph for KP52 + 750; (d) regression graph for KP52 + 750; (e) line graph for KP04 + 900; (f) regression graph for KP04 + 900; (g) line graph for KP35 + 050; (h) regression graph for KP35 + 050.

agricultural, semi-desert areas (barelands), grasslands, industrial, residential areas, mud volcanoes and water. Inclusion of the NDBI, Urban Index, NDVI, NDMI, SAVI, NDWI and Iron Oxide significantly contribute to the segmentation of the satellite images with the accurate spectral separation of segments and accurate boundary localization prior to the classification (Yuan et al. 2014). Total number of computed segments was **28979** out of which 1500 were collected as training segments/samples for the classification purposes. Error (confusion/contingency) matrix of the developed landcover along pipelines is presented in Table 2 and it is possible to observe that the

Table 2. Error (confusion/contingency) matrix of classified land-cover along petroleum and gas pipelines.

		Reference Data								
	LANDCOVER	Agricultural	Grasslands	Residential Areas	Semi-desert areas	Industrial	Mud Volcanoes	Water	Total	User's accuracy (%)
Classified Data	Agricultural	139	16	2	5	0	0	3	165	84%
	Grasslands	6	184	0	44	0	0	0	234	79%
	Residential Areas	3	2	59	0	1	0	0	65	91%
	Semi-desert areas (Bare-lands)	0	44	1	80	0	0	0	125	64%
	Industrial	0	0	0	0	10	0	0	10	100%
	Mud Volcanoes	0	0	0	0	0	12	0	12	100%
	Water	3	1	0	2	0	0	33	39	85%
	Total	151	247	62	131	11	12	36	650	
	Producer's accuracy	92%	74%	95%	61%	91%	100%	92%		
	Overall Accuracy									80%

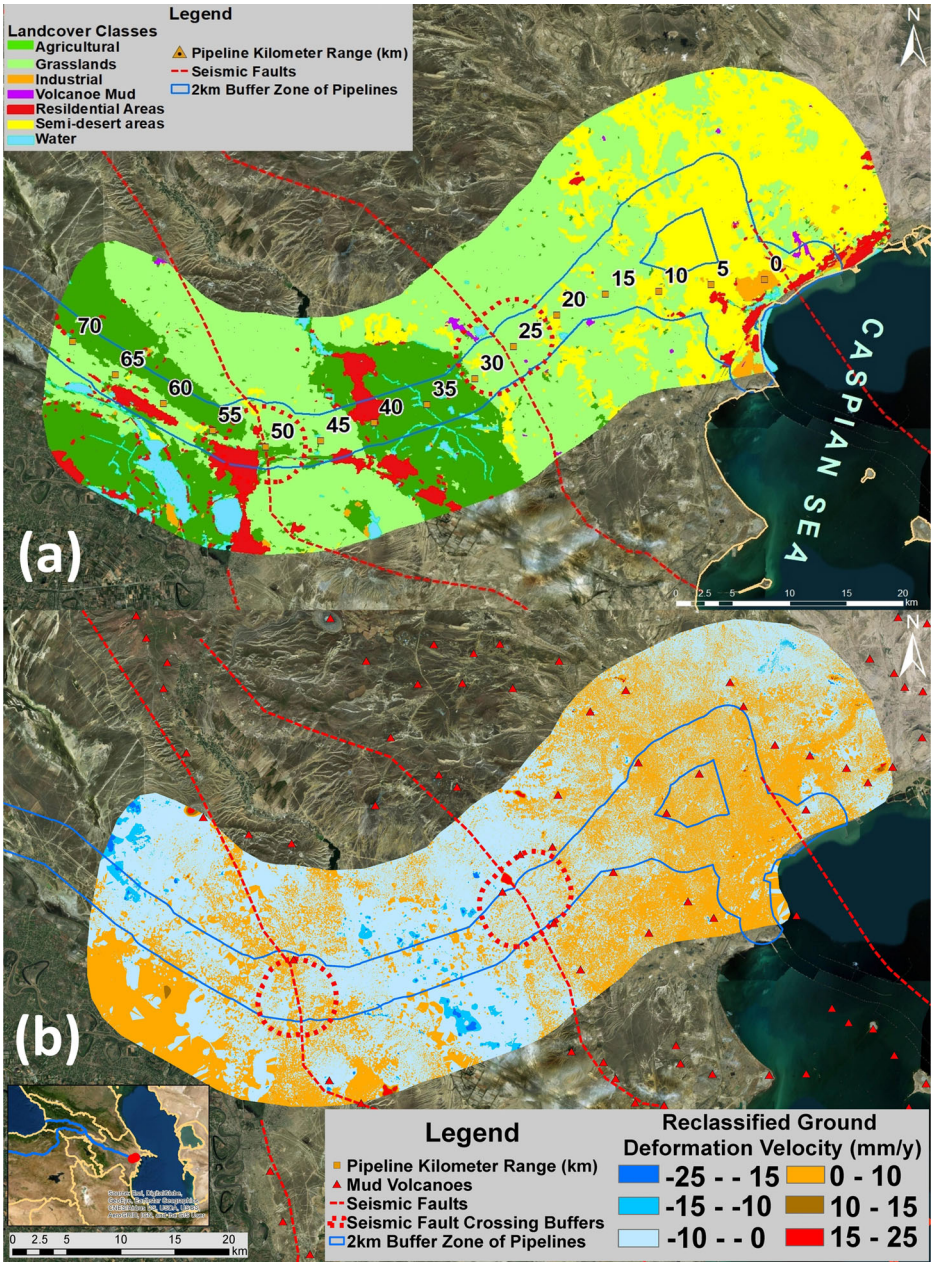

Figure 12. (a) Landcover map; (b) reclassified ground velocity along petroleum and gas pipelines.

overall accuracy of classification validated with the use of 650 control points is 80%. The classification model primarily confused between the semi-desert areas (barelands) and grasslands even though the NDVI spectral index was included into the segmentation process. The landcover developed using OBIA approach (Figure 12a) and reclassified PS-InSAR ground deformation velocity (Figure 12b) allowed to quantify the ground deformation velocities within the landcover classes for the analysis of the

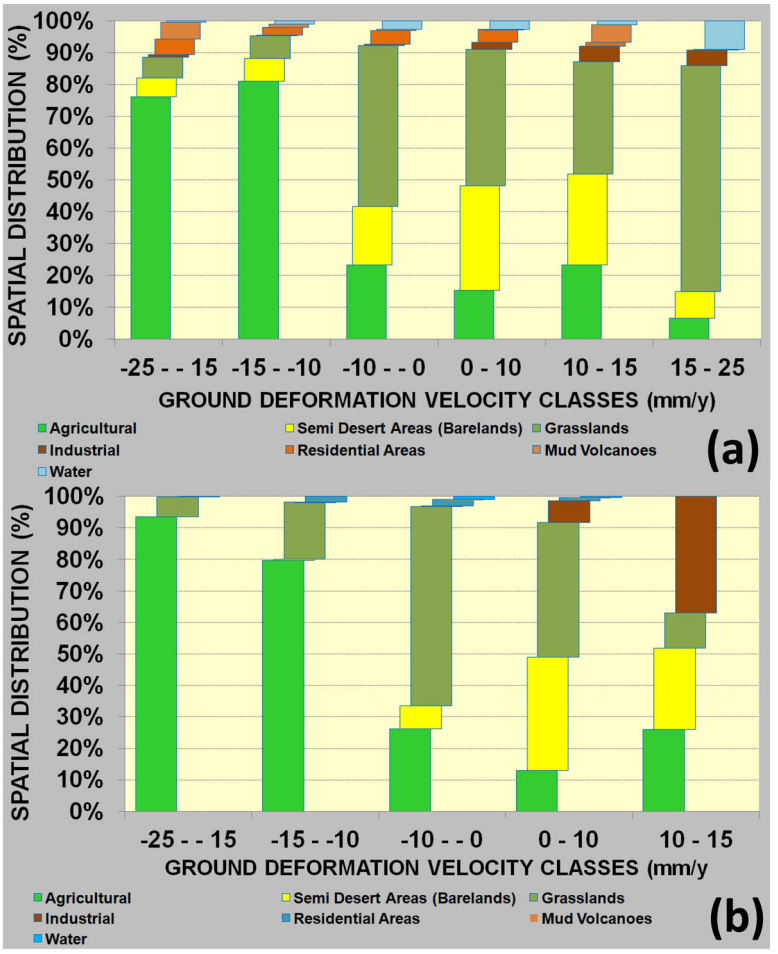

Figure 13. Spatial distribution of ground deformation velocity within the landcover classes (a) within 10 km buffer zone; (b) within 250 m buffer zone.

spatial distribution (Figures 13a and 13b). In Figure 4a–f, most subsiding KP30-45 and KP60-72 pipeline ranges cross the agricultural lands, whereas uplifting KP0-13 pipeline range cross the semi-desert barelands with a number of mud volcanoes. The spatial trends of ground subsidence and uplifts allow to conclude that there is obviously a primary controlling factor of natural tectonic impacts. As follows from Figure 1a, this natural tectonic factor is also reflected in the majority of earthquakes and mud volcanoes located along the seismic faults. Nevertheless, the subsidence hotspots (KP30-45 and KP60-72) are crossed by croplands and this allows to assume that agricultural activities like overuse of groundwater, irrigation and ploughing etc. are also secondary controlling factors of subsidence processes along petroleum and gas pipelines. This is also reflected in Figures 13a and 13b where the largest spatial distribution of subsidence velocity class (-25 - – 15) was prevailing within the agricultural landcover class along oil and gas pipelines with the 10 km and 250 m buffer zones, respectively.

4. Discussion

These studies demonstrated the practical values for the measurements of ground deformation velocity and rates using PS-InSAR along the corridor of underground oil and gas pipelines. The outcomes of this research suggests that the PS-InSAR technique can have a high potential for the optimized and simplified monitoring and risk management of ground deformations along pipelines, but the use of only this technique for the assessment of ground movement risks to petroleum and gas infrastructure needs to be carefully evaluated (Tofani et al. 2013). Since the BTC, SCP, SCPX and WREP pipelines are underground, for the present studies it was obviously impossible to judge about the conditions of the pipelines in terms of any kind of deformations but it was only feasible to analyze the status of ground movements. Even if the PSI technique can be used as the predictor for the prioritization of potential risky sites, it cannot fully replace in-situ measurements based on the visual inspections and geodetic measurements. The justification of remediation costs requires detailed geotechnical assessments on the ground with the consideration of geodetic measurements, readings from piezometers, inclinometers, pipeline in-line inspections like different types of piggings, direct current voltage gradient (dcvg) and close interval potential surveys, depth of pipelines, existing trapezoidal trench standards etc. to understand how seriously pipelines are affected. If there are no specific changes in the shape of pipelines and other conditions, then this will raise a number of questions in terms of probability of failure for the evaluation prior to the investment into the geotechnical remediation activities. It is also necessary to emphasize the availability of historical recordings of actual pipelines incidents caused by the ground deformation processes.

However, very often for the sites of interest, there are no historical records from geodetic measurements to set-up a baseline for the continuous site monitoring. In this case time-series of space satellite observations are irreplaceable. It is also necessary to emphasize that the single-point measurements using ground-based geodetic techniques are not sufficient to analyze broader spatial patterns of ground movements.

Even though there are many studies focused on PS-InSAR, the present research demonstrated the combined PS-InSAR and the geospatial machine learning – based interpolation and concentration analysis which contributed to the development and understanding of the broader picture of ground deformation processes along petroleum and gas pipelines. Majority of PS-InSAR studies primarily analyzed and summarized produced results using generated point clouds of ground movement velocity and rates. However this research clearly demonstrated that running of advanced spatial interpolation and concentration statistics would significantly contribute to more comprehensive research results.

PS-InSAR studies showed the prevailing and continuous subsidence patterns in the KP13-70 range of pipelines crossing two active seismic faults. The ground uplift deformations were observed in the pipeline range of KP0-KP13. The spatial distribution of sites with ground deformation velocity less than − 15 mm/y and more than 15 mm/y was diverse and random all along 70 km of pipelines without any cumulative spatial patterns. This means that it would be complicated to find all of these locations using purely ground-based expeditions and visual inspections.

Even though PS-InSAR demonstrated a reliable approach for the detection of ground deformation processes along petroleum and gas pipelines, it is highly recommended to advance these studies with the integration of other geological, geotechnical, seismic, thermal and climatic information to better understand controlling natural and man-made factors. Besides, it is crucial to also use other techniques like Small Baseline Subset (SBAS), Intermittent Small Baseline Subset (ISBAS) and SqueeSAR and cross-validate measured results (Sowter et al. 2013; Gee et al. 2016; Sowter et al. 2016; Gee et al. 2017; Sowter et al. 2018).

To the extent of our awareness, for the present study area of BTC, SCP, SCPX and WREP pipelines, these studies of public accessibility is the first in a sequence of works that seeks to answer whether or not PS-InSAR - based technique holds practical value for the pipeline operators to highlight areas of ground deformations at seismic faults and also along entire range of pipelines. However, the erosion vulnerability of these pipelines was well studied by Bayramov 2013 using the optical multi-temporal remote sensing. These studies concluded that first 70 km of BTC, SCP, SCPX and WREP pipelines are most vulnerable to erosion occurrences which create risks of pipeline damage by natural and anthropogenic factors. In particular this was related to the soil types with high silt content, low vegetation cover and hilly terrain. This means that there is obviously an impact from ground deformation processes which should also be investigated in the spatial relationship to naturally occurred erosion processes along petroleum and gas pipelines. Based on the pipeline related studies by Hole et al. 2011, it is recommended to run PS-InSAR in both ascending and descending acquisition models to resolve the LOS measurements into vertical deformation. Vertical displacement can only be estimated from a single LOS measurement if motion azimuth and the angle between slope motion and a level plane are assumed for the area of interest (Hole et al. 2011). As it was mentioned before in the present studies it was not feasible to perform computations for both ascending and descending acquisitions because of nonsufficient computing power and storage space. Therefore single LOS measurements were obtained from the descending flight direction and approximated to the vertical movement as proposed by Dai et al. (2015), Gee et al. (2016) and Hole et al. (2011). Singhroy et al. (2018) used the corner reflectors along buried oil pipelines to detect subtle ground and pipeline movements, thereby reduced the need for frequent ground based survey campaigns and increased the reliability, precision and confidence level of measurements. Sharma et al. (2016) coupled the InSAR displacements, GIS analyses, field data and geomechanical modelling to optimize understanding of landslide geohazards along pipelines. Ianoschi et al. (2013) determined the feasibility of gas pipeline monitoring by PS-InSAR using TerraSAR-X (3×3 m) radar satellite images and application of high resolution images added significant amount of information and details in terms of point density. Considering fore-mentioned InSAR studies along pipelines, it is possible to conclude that for the best performance of PS-InSAR techniques along petroleum and gas pipelines, it is necessary: to process both ascending and descending passes for the computation of precise vertical movement; install permanent corner reflectors along vulnerable areas of pipeline movements and also areas with a lack of objects of high scattering properties for the reliability, precision and confidence of measurements; apply both high and low resolution radar images; collect all possible geological and geotechnical contextual information from

ground-based surveys and other sources to perform combined analysis; run other SAR ground deformation techniques to cross-validate the results. Another limitation is to automate separation of natural - and manmade - caused ground changes which can be mistakenly reflected as the subsidence or uplift, e.g., development of petroleum and gas infrastructure or excavation activities etc. Ianoschi et al. 2013 performed PS-InSAR with further classification and characterization of persistent scatterers (PS) in terms of ground or building reflections. The thresholding approach was used to perform this classification (Dheenathayalan and Hanssen 2011; Dheenathayalan et al. 2011). This is crucial to effectively prioritize critical points for further field investigations along petroleum and gas pipelines. Therefore, it is necessary to proceed with the present studies by applying of other advanced ground movement measurement techniques. It is also necessary to integrate more geospatial information to understand natural and man-made controlling factors of ground movement processes and improve the reliability of produced results.

5. Conclusions

We performed PS-InSAR analysis along petroleum and gas pipelines to identify the spatial patterns of ground surface deformations with respect to the location of active seismic faults. Our conclusions are as follows:

1. As a primary factor of ground deformations, the influence of tectonic movements was observed in the broad-scale analysis along 70 km long and 10 km wide section of petroleum and gas pipelines with the prevailing and continuous subsidence in the KP13-70 range of pipelines crossing two active seismic faults. However the largest subsidence rates were observed in the areas of croplands, where agricultural activities like overuse of groundwater, irrigation and ploughing etc. also negatively affect to the ground movement processes along pipelines as the secondary factor. The ground uplift deformations were observed in the pipeline range of KP0-KP13. The largest spatial distribution of subsidence velocity class (-25 - - 15) was prevailing within the agricultural landcover class along oil and gas pipelines.
2. Local-scale analyses were performed along 70 km section of pipelines with 250m buffer zone for the detailed quantitative ground movement assessment of two seismic faults. The minimum and maximum vertical ground movement velocities were observed to be -21.3 mm/y and 14.1 mm/y. The minimum and maximum ground movement rates in December **27, 2019** since January **6, 2018** were observed to be -46.09 mm and 33.46 mm, respectively. Both of them were observed within the buffer zones of two seismic faults. However, the spatial distribution of sites with ground deformation velocity less than - 15mm/y and more than 15mm/y was diverse and random all along 70 km of pipelines without any cumulative spatial patterns.
3. Seismic Fault KP21-31 revealed its higher vulnerability to subsidence processes rather than the Seismic Fault KP46-54 and this was reflected in lower mean, variation and standard deviation of pixel values the buffer zones of seismic faults with 250m width. The ground deformation velocities within the range of Seismic Fault KP21-31 revealed the minimum and maximum values of -19.74 mm/y and 14.1mm/y, respectively. The minimum and maximum ground movement rates in

December **27, 2019** since January **6, 2018,** were observed to be - 46.07mm and 33.46mm. The ground deformation velocities within the Seismic Fault KP46-54 revealed the minimum and maximum values of -17.07mm/y and 9.29mm/y. The minimum and maximum ground movement rates in December **27, 2019** since January **6, 2018,** were observed to be -46.09mm and 22.24mm.

4. Encouraging level of agreement with the regression coefficients of 0.92 and 0.96 for known subsiding sites at KP28 + 500 and KP52 + 750 respectively was observed between the high-precision GPS and PS-InSAR measurements. It was also possible to observe the encouraging level of correlation between the high-precision GPS and PS-InSAR measurements with the regression coefficients of 0.97 and 0.96 for known uplifting sites at KP04 + 900 and KP35 + 050, respectively. Although the GPS measurements showed minor variations in comparison to PS-InSAR (RMSE of 2.7mm and 2.5 mm for KP28 + 500 and KP52 + 750 respectively; the RMSE of 1.7 mm and 1.9 mm for KP04 + 900 and KP35 + 050) the achieved accuracy allows to state without any doubts that the deformation trends clearly confirms the presence of subsidence processes at the seismic faults. This means that the PS-InSAR – based approach outlined in this paper is a significant improvement over current ground-based monitoring practices.
5. The spatial distribution and variation of ground movement processes along pipelines demonstrated that general geological and geotechnical understanding of the study area is not sufficient to find and mitigate all the critical areas of subsidence and uplifts for the pipeline operators. The prediction of the potential subsidence or uplift locations based on the field visual verifications holds a lot of uncertainties without broad and detailed scale airborne, satellite or unmanned aerial vehicle space observation technologies. The justification of the budget for the geotechnical maintenance activities along long-range oil and gas pipelines requires sophisticated prioritization and planning of the remediation sites and clear quantitative and qualitative risk assessment proving the activeness of these sites and effectiveness of the remediation measures.
6. Even though PS-InSAR demonstrated a reliable approach for the detection of ground deformation processes along petroleum and gas pipelines, it is highly recommended to advance these studies with the integration of other geological, geotechnical, thermal and climatic information to better understand controlling natural and man-made factors. Besides, it is crucial to also use other techniques like Small Baseline Subset (SBAS), Intermittent Small Baseline Subset (ISBAS) and SqueeSAR and cross-validate the results.

Disclosure statement

No potential conflict of interest was reported by the authors.

Acknowledgements

The authors would like to thank Nazarbayev University.

Funding

This research has been funded by the Nazarbayev University through the Faculty-development Competitive Research Grant (FDCRGP) - Funder Project Reference: 080420FD1917.

References

Chang L, Ku O, Hanssen RF. 2019. Identification of deformation pattern changes caused by enhanced oil recovery (EOR) using InSAR. Int J Remote Sens. 40(4):1495–1505.

Gee D, Bateson L, Sowter A, Grebby S, Novellino A, Cigna F, Marsh S, Banton C, Wyatt L. 2017. Ground motion in areas of abandoned mining: application of the Intermittent SBAS (ISBAS) to the Northumberland and Durham Coalfield, UK. Geosciences. 7(3):85.

Aslan G, Cakir Z, Lasserre C, Renard F. 2019. Investigating subsidence in the Bursa Plain, Turkey, using ascending and descending Sentinel-1 satellite data. Remote Sens. 11(1):85.

Bayramov ER. 2013. Quantitative assessment of vegetation renaturation and soil degradation and their control by climate and ground factors along rights-of-way of petroleum/gas pipelines, Azerbaijan. [PhD Dissertation]. Dresden, Germany: Dresden University of Technology.

Bonì R, Bosino A, Meisina C, Novellino A, Bateson L, McCormack HA. 2018. Methodology to detect and characterize uplift phenomena in urban areas using Sentinel-1 data. Remote Sens. 10(4):607.

Chang L, Dollevoet RPBJ, Hanssen RF. 2018. Monitoring line-infrastructure with multisensor SAR interferometry: products and performance assessment metrics. IEEE J Sel Top Appl Earth Obs Remote Sens. 11(5):1593–1605.

Cleve C, Kelly M, Kearns FR, Moritz M. 2008. Classification of the wildland–urban interface: a comparison of pixel- and object based classifications using high-resolution aerial photography. Comput Environ Urban Syst. 32(4):317–326.

Colesanti C, Ferretti A, Novali F, Prati C, Rocca F. 2003. SAR monitoring of progressive and seasonal ground deformation using the permanent scatterers technique. IEEE Trans Geosci Remote Sens. 41(7):1685–1701.

Dai KR, Liu GX, Li ZH, Li T, Yu B, Wang XW, Singleton A. 2015. Extracting vertical displacement rates in Shanghai (China) with multi-platform SAR images. Remote Sens. 7(8): 9542–9562.

D'Aria D, Ferretti A, Guarnieri AM, Tebaldini S. 2010. SAR calibration aided by permanent scatterers. IEEE Trans Geosci Remote Sens. 48(4):2076–2086.

Dehvari A, Heck RJ. 2009. Comparison of object-based and pixel based infrared airborne image classification methods using DEM thematic layer. J Geogr Reg Plan. 2(4):086–096.

Dheenathayalan P, Caro Cuenca M, Hanssen RF. 2011b. Different approaches for psi target characterization for monitoring urban infrastructure. In: 8th International Workshop on Advances in the Science and Applications of SAR Interferometry, 'FRINGE 2011', Frascati, Italy; Sep 2011. ESA. p. 19–23.

Dheenathayalan P, Hanssen R. 2011a. Target characterization and interpretation of deformation using persistent scatterer interferometry and polarimetry. In: 5th International Workshop on Science and Applications of SAR Polarimetry and Polarimetric Interferometry, 'POLInSAR 2011; Jan 2011, Frascati, Italy. p. 24–28.

Dupuy S, Barbe E, Balestrat M. 2012. An object-based image analysis method for monitoring land conversion by artificial sprawl use of RapidEye and IRS data. Remote Sens. 4(2): 404–423.

Durieux L, Lagabrielle E, Nelson A. 2008. A method for monitoring building construction in urban sprawl areas using object-based analysis of SPOT 5 images and existing GIS data. ISPRS J Photogramm Remote Sens. 63(4):399–408.

Environmental Systems Research Institute (ESRI). 2014a. ArcGIS Pro Help. https://pro.arcgis.com/en/pro-app/tool-reference/spatial-analyst/point-density.htm.
Environmental Systems Research Institute (ESRI). 2014b. ArcGIS Pro Help. https://pro.arcgis.com/en/pro-app/tool-reference/spatial-analyst/trend.htm.
Farr TG, Rosen PA, Caro E, Crippen R, Duren R, Hensley S, Kobrick M, Paller M, Rodriguez E, Roth L, et al. 2007. The shuttle radar topography mission. Rev Geophys. 45(2):RG2004.
Ferretti A, Bianchi M, Prati C, Rocca F. 2005. Higher-order permanent scatterers analysis. EURASIP J Adv Signal Process. 2005(20):609604.
Ferretti A, Fumagalli A, Novali F, Prati C, Rocca F, Rucci A. 2011. A new algorithm for processing interferometric data-stacks: SqueeSAR. IEEE Trans Geosci Remote Sens. 49(9): 3460–3470.
Ferretti A, Prati C, Rocca F. 2000. Nonlinear subsidence rate estimation using permanent scatterers in differential SAR interferometry. IEEE Trans Geosci Remote Sens. 38(5):2202– 2212.
Ferretti A, Prati C, Rocca F. 2001. Permanent scatterers in SAR interferometry. IEEE Trans Geosci Remote Sens. 39(1):8–20.
Ferretti A, Savio G, Barzaghi R, Borghi A, Musazzi S, Novali F, Prati C, Rocca F. 2007. Submillimeter accuracy of InSAR time series: experimental validation. IEEE Trans Geosci Remote Sens. 45(5):1142–1153.
Gee D, Sowter A, Novellino A, Marsh S, Gluyas J. 2016. Monitoring land motion due to natural gas extraction: validation of the intermittent SBAS (ISBAS) DInSAR algorithm over gas fields of North Holland, the Netherlands. Mar Pet Geol. 77:1338–1354.
Grebby S, Orynbassarova E, Sowter A, Gee D, Athab A. 2019. Delineating ground deformation over the Tengiz oil field, Kazakhstan, using the intermittent SBAS (ISBAS) DInSAR algorithm. Int J Appl Earth Obs Geoinf. 81:37–46.
Guthrie R, Reid E, Richmond J, Ghuman P, Cormier Y. 2018. InSAR and the pipeline geohazards toolbox: instructions for use as of 2018. Proceedings of **2018 12**th International Pipeline Conference; Sep 24–**28, 2018**; Calgary, Alberta, Canada.
Hole J, Holley R, Giunta G, Lorenzo G, Thomas A. 2011. InSAR assessment of pipeline stability using compact active transponders. Proceedings of Fringe 2011, Sep 19–23; Frascati, Italy; ESA SP-697. p. 53.
Honglei Y, Jun-Huan P. 2015. Monitoring urban subsidence with multi-master radar interferometry based on coherent targets. J Indian Soc Remote Sens. 43(3):529–538.
Hooper A, Zebker H, Segall P, Kampes B. 2004. A new method for measuring deformation on volcanoes and other natural terrains using InSAR persistent scatterers. Geophys Res Lett. 31(23):L23611.
Ianoschi R, Schouten M, Leezenberg PB, Dheenathayalan P, Hanssen R. 2013. Satellite radar interferometry for risk management of gas pipeline networks. Proc. 'ESA Living Planet Symposium 2013'; Sep. 9–13 (ESA SP-722), Edinburgh, UK.
Imamoglu M, Kahraman F, Cakir Z, Sanli FB. 2019. Ground deformation analysis of Bolvadin (W. Turkey) by means of multi-temporal InSAR techniques and Sentinel-1 data. Remote Sens. 11(9):1069.
Ivits E, Koch B, Blaschke T, Jochum M, Adler P. 2005. Landscape structure assessment with image grey-values and object-based classification at three spatial resolutions. Int J Remote Sens. 26(14):2975–2993.
Ji L, Zhang Y, Wang Q, Xin Y, Li J. 2016. Detecting land uplift associated with enhanced oil recovery using InSAR in the Karamay oil field, Xinjiang, China. Int J Remote Sens. 37(7): 1527–1540.
Kampes B. 2005. Displacement parameter estimation using permanent scatterer interferometry [PhD thesis]. Delft, the Netherlands: Delft University of Technology.
Liu D, Xia F. 2010. Assessing object-based classification: advantages and limitations. Remote Sensing Letters. 1(4):187–194.
Liu Y, Huang H, Liu Y, Bi H. 2016. Linking land subsidence over the Yellow River delta, China, to hydrocarbon exploitation using multi-temporal InSAR. Nat Hazards. 84(1): 271–291.

Lu L, Liao M. 2008. Subsidence measurement with ps-insar techniques in Shanghai urban. The International Archives of the Photogrammetry, Remote Sensing and Spatial Information Sciences. Vol. XXXVII. Part B7. Beijing.

Matinfar HR, Sarmadian F, Alavi Panah SK, Heck RJ. 2007. Comparisons of object-oriented and pixel-based classification of land use/land cover types based on Lansadsat7 ETM? Spectral bands (case study: arid region of Iran). Am Eurasian J Agric Environ Sci. 2(4): 448–456.

Mikhailov VO, Kiseleva EA, Smol'yaninova EI, Dmitriev PN, Golubev VI, Timoshkina EP, Khairetdinov SA. 2018. Satellite radar interferometry: new technologies for satellite monitoring of mining areas and displacements of natural and man-made objects. Seism Instr. 54(5): 515–520.

Myint SW, Gober P, Brazel A, Grossman-Clarke S, Weng Q. 2011. Per-pixel vs. object-based classification of urban land cover extraction using high spatial resolution imagery. Remote Sens Environ. 115(5):1145–1161.

Osmanoğlu B, Sunar F, Wdowinski S, Cabral-Cano E. 2016. Time series analysis of InSAR data: Methods and trends. ISPRS J Photogramm Remote Sens. 115:90–102.

Perissin D, Ferretti A. 2007. Urban-target recognition by means of repeated spaceborne SAR images. IEEE Trans Geosci Remote Sens. 45(12):4043– 4058.

Ru W, Tianliang Y, Mengshi Y, Mingsheng L, Jinxin L. 2019. A safety analysis of elevated highways in Shanghai linked to dynamic load using long-term time-series of InSAR stacks. Remote Sens Lett. 10(12):1133–1142.

Rucker ML, Panda BB, Meyers RA, Lommler JC. 2013. Using InSAR to detect subsidence at brine wells, sinkhole sites, and mines. Carbonates Evaporites. 28(1–2):141–147.

Sande CJ, Jong SM, Roo APJ. 2003. A segmentation and classification approach of IKONOS-2 imagery for land cover mapping to assist flood risk and flood damage assessment. Int J Appl Earth Obs Geoinform. 4:217–229.

Sharma J, Busler J, Francioni M, Stead D, Donati D, Onsel E, Clague J, Brideau MA. 2016. Monitoring landslides along pipeline corridors using a combined satellite-based InSAR and geomechanical modelling approach. In: Proceedings of GeoVancouver 2016.

Shi J, Yang H, Peng J, Wu L, Xu B, Liu Y, Zhao B. 2019. InSAR monitoring and analysis of ground deformation due to fluid or gas injection in fengcheng oil field, Xinjiang, China. J Indian Soc Remote Sens. 47(3):455–466.

Singhroy V, Alasset P, Couture R and Poncos V. 2007. InSAR monitoring of landslides on permafrost terrain in canada, IEEE International Geoscience and Remote Sensing Symposium, Barcelona, 2007, pp. 2451–2454, doi: 10.1109/IGARSS.2007.4423338.

Singhroy V, Li J, Blais-Stevens A, Fobert M-A. 2018. Insar monitoring of pipeline routes. IGARSS 2018 - 2018 IEEE International Geoscience and Remote Sensing Symposium, Valencia. p. 212–215

Singhroy V, Li J, Charbonneau F. 2015. High resolution rapid revisit InSAR monitoring of surface deformation. Can J Remote Sens. 41(5):458–472.

Sircar S, Power D, Randell C, Youden J, Gill E. 2004. Lateral and subsidence movement estimation using InSAR. Proc. of the 2004 IGARSS; Sep 20–24, Anchorage, Alaska; Vol. 5. p. 2991–2994.

Solari L, Bianchini S, Franceschini R, Barra A, Monserrat O, Thuegaz P, Bertolo D, Crosetto M, Catani F. 2020. Satellite interferometric data for landslide intensity evaluation in mountainous regions. Int J Appl Earth Obs Geoinf. 87 (2020):102028.

Sowter A, Athab A, Novellino A, Grebby S, Gee D. 2018. Supporting energy regulation by monitoring land motion on a regional and national scale: a case study of Scotland. Proc Inst Mech Eng Part A J Power Energy. 232(1):85–99.

Sowter A, Bateson L, Strange P, Ambrose K, Syafiudin M. 2013. DInSAR estimation of land motion using intermittent coherence with application to the South Derbyshire and Leicestershire coalfield. Remote Sens Lett. 4 (10):979–987.

Sowter A, Che Amat M, Cigna F, Marsh S, Athab A, Alshammari L. 2016. Mexico City land subsidence in 2014–2015 with sentinel-1 IW TOPS: results using the Intermittent SBAS (ISBAS) technique. Int J Appl Earth Obs Geoinf. 52:230–242.

Tofani V, Raspini F, Catani F, Casagli N. 2013. Persistent scatterer interferometry (PSI) technique for landslide characterization and monitoring. Remote Sens. 5(3):1045–1065.

Wasowski J, Bovenga F, Nutricato R, Nitti DO, Chiaradia MT. 2018. Advanced satellite radar interferometry for deformation monitoring and infrastructure control in open-cast mines and oil/gas fields. Innov Infrastruct Solut. 3(68):1-7.

Whiteside TG, Boggs GS, Maier SW. 2011. Comparing object-based and pixel-based classifications for mapping savannas. Int J Appl Earth Obs Geoinf. 13(6):884–893.

Yan G, Mas JF, Maathuis B, Xiangmin Z, Van Dijk P. 2006. Comparison of pixel-based and object-oriented image classification approaches: a case study in a coal fire area, Wuda, Inner Mongolia, China. Int J Remote Sens. 27(18):4039–4055.

Yan S, Shi K, Li Y, Liu J, Zhao H. 2020. Integration of satellite remote sensing data in underground coal fire detection: a case study of the Fukang region, Xinjiang, China. Front Earth Sci. 14(1):1–12.

Yang C, Zhang D, Zhao C, Han B, Sun R, Du J, Chen L. 2019. Ground deformation revealed by Sentinel-1 MSBAS-InSAR time-series over karamay oilfield, China. Remote Sens. 11(17):2027.

Yuan J, Wang D, Li R. 2014. Remote sensing image segmentation by combining spectral and texture features. IEEE Trans Geosci Remote Sens. 52(1):16–24.

Yunjun Z, Fattahi H, Amelung F. 2019. Small baseline InSAR time series analysis: unwrapping error correction and noise reduction. Comput Geosci. 133:104331.

Zhang A, Lu J, Kim JW. 2018. Detecting mining-induced ground deformation and associated hazards using spaceborne InSAR techniques. Geomatics Nat Hazards Risk. 9(1):211–223.

Zhang Q, Li Y, Zhang J, Luo Y. 2019. InSAR technique applied to the monitoring of the Qinghai–Tibet Railway. Nat Hazards Earth Syst Sci. 19(10):2229–2240.

Zheng M, Deng K, Du S, Liu J, Liu J, Feng J. 2019. Joint probability integral method and TCPInSAR for monitoring mining time-series deformation. J Indian Soc Remote Sens. 47(1):63–75.